Applied Materials Today 41 (2024) 102464

Contents lists available at ScienceDirect

Applied Materials Today

journal homepage: www.elsevier.com/locate/apmt

$Ti_3C_2T_x$ and $Mo_2TiC_2T_x$ MXenes as additives in synovial fluids - towards an enhanced biotribological performance of 3D-printed implants

Max Marian [a,b,*], Cotty D. Quiroz Esteban [c], Dario F. Zambrano [c], Sangharatna M. Ramteke [b], Jorge Ramos Grez [b], Brian C. Wyatt [d,e], Jacob Patenaude [d], Bethany G. Wright [d], Babak Anasori [d,e], Andreas Rosenkranz [c,f,*]

[a] Institute for Machine Design and Tribology (IMKT), Leibniz University Hannover, Garbsen, Germany
[b] Department of Mechanical and Metallurgical Engineering, School of Engineering, Pontificia Universidad Católica de Chile, Santiago, Chile
[c] Department of Chemical Engineering, Biotechnology and Materials (FCFM), Universidad de Chile, Santiago, Chile
[d] School of Mechanical Engineering, Purdue University, West Lafayette, United States
[e] School of Materials Engineering, Purdue University, West Lafayette, United States
[f] ANID – Millennium Science Initiative Program, Millennium Nuclei of Advanced MXenes for Sustainable Applications (AMXSA), Santiago, Chile

ARTICLE INFO

Keywords:
2D materials
MXenes
Biotribology
Wear resistance
Additive manufacturing

ABSTRACT

Synovial joints, critical for limb biomechanics, rely on sophisticated lubrication systems to minimize wear. Disruptions, whether from injury or disease, often necessitate joint replacements. While additive manufacturing offers personalized implants, ensuring wear resistance remains a challenge. This study delves into the potential of $Ti_3C_2T_x$ and $Mo_2TiC_2T_x$ nanosheets in mitigating wear of additively manufactured cobalt-chromium tungsten alloy substrates when incorporated as additives into synovial fluid. The colloidal solutions demonstrate an excellent stability, a crucial factor for reproducible assays and potential clinical applicability. Analysis of contact angles and surface tensions reveals MXene-induced alterations in substrate wettability, while maintaining their general hydrophilic character. Viscosity analysis indicates that MXene addition reduces the dynamic viscosity, particularly at higher concentrations above 5 mg/mL, thus enhancing dispersion and lubrication properties. Friction and wear tests demonstrate a dependency on the MXene concentration, while $Ti_3C_2T_x$ exhibits stable friction coefficients and up to 77 % wear reduction at 5 mg/mL, which was attributed to the formation of a wear-protecting tribo-film (amorphous carbon and MXene nano-sheets). Our findings suggest that $Ti_3C_2T_x$, when supplied in favorable concentrations, holds promise for reducing wear in biotribological applications, offering avenues for future research into optimizing MXene utilization in load-bearing joint replacements and other biomedical devices.

1. Introduction

The human body comprises intricate sets of living tissues with numerous contact interfaces, which are typically lubricated by vital body fluids. Among these, synovial joints stand out as pivotal components in limb biomechanics, which facilitate the movement of rigid structures like bones. The integrity of synovial joints relies on a delicate interplay of anatomical and cellular components, namely featuring the synovial fluid (SF). This viscous fluid, which is composed of plasma proteins, cellular elements, and lubricating molecules, among other substances, is essential for the maintenance and regulation of physiological processes [1,2]. The disruption in these lubrication systems, whether due to injury, disease, or aging, increases friction and wear, which can lead to irreversible damages and often joint replacement with prosthetic devices, a commonplace medical procedure today. However, the removal of the generated wear debris from these articulating surfaces during usage can result in complications, including metallosis, tissue inflammation, osteolysis, implant loosening, and eventual failure [3,4]. Hence, the biotribological behavior of these systems becomes paramount for their safe and reliable operation. The limited effectiveness of existing solutions imposes a significant financial burden on healthcare systems and subjects patients to prolonged

* Corresponding authors.
E-mail addresses: marian@imkt.uni-hannover.de (M. Marian), sangharanta.ramteke@uc.cl (S.M. Ramteke), jramos@uc.cl (J.R. Grez), wyatt2@purdue.edu (B.C. Wyatt), jpatena@purdue.edu (J. Patenaude), bgwright@iu.edu (B.G. Wright), banasori@purdue.edu (B. Anasori), arosenkranz@ing.uchile.cl (A. Rosenkranz).

https://doi.org/10.1016/j.apmt.2024.102464
Received 24 May 2024; Received in revised form 25 September 2024; Accepted 1 October 2024
Available online 7 October 2024

suffering, leading to revision surgeries [5].

Metals, such stainless steel, titanium (Ti) or cobalt-chromium (CoCr) alloys have found extensive use in medical devices due to their overall biocompatibility combined with their tensile strength, fracture toughness, and overall durability, making them suitable for load-bearing joint replacements like total hip or total knee arthroplasty [6–8]. Nevertheless, the release of metallic and oxide wear debris into the peri-implant space can trigger various adverse biochemical reactions, ranging from localized inflammation and bone loss to toxic effects, implant contamination, and mechanical failure [5].

Additive manufacturing (AM) of metals presents a promising avenue for load-bearing joint replacements, offering the potential for complex, patient-specific designs that optimize fit and functionality. This technology can revolutionize this field by reducing reliance on off-the-shelf implants and potentially enhancing patients' comfort and mobility, as these are precisely made to fit the specific anatomy. However, a significant challenge relates to the wear resistance of AM parts [9]. Traditional manufacturing methods often employ specialized materials and processes to meet rigorous wear requirements for load-bearing joints, whereas AM materials may fall short in this regard. Overcoming this limitation is a critical focus for researchers and engineers to ensure the long-term success and safety of additively manufactured joint implants.

In the realm of tribology, 2D layered materials hold tremendous potential to reduce friction and wear in various substrate materials, whether operating under dry or lubricated conditions [10,11]. Current research endeavors are geared towards the development of materials with low friction, minimal wear, and corrosion resistance. In this regard, two-dimensional (2D) materials, such as graphene and its derivatives, transition metal dichalcogenides, and hexagonal boron nitride (*h*-BN), have garnered notable attention due to their high mobility, excellent electrical conductivity, fair mechanical strength, and extended spin diffusion length. When used as additives in lubricated systems, 2D materials serve various functions within the contact area [12]. They can act as shearing films and nano-roller bearings during sliding, which potentially transitions the friction mechanism from sliding to rolling, while also regulating the lubricant flow to minimize frictional losses [11, 13]. Regardless of the dry or lubricated nature of the contact, 2D materials may initiate tribo-chemical reactions [14], which lead to the formation of advantageous tribo-films with low shear resistance [15]. Due to their weak interlayer interactions, these tribo-films can transfer onto the tribological counter-body during rubbing, forming a tribo-layer/tribo-layer interface with enhanced tribological properties.

The potential utility of 2D materials in biomedical applications is underscored by their advantageous properties in terms of layered structure, closely spaced interlayers, and elevated specific surface areas [16,17]. This characteristic can be harnessed for purposes such as adsorption, enhancing adhesion, or chemical functionalization. Regarding biomedical applications, 2D materials exhibit intrinsic biocompatibility with antibacterial and antiviral properties, making them suitable for various biomedical applications [18,19].

Consequently, they also have the potential to revolutionize the design and performance of load-bearing implants, either as protective coatings to suppress substrate wear debris generation without affecting bulk properties or as fillers in composites to enhance mechanical properties [18,20]. Regarding metallic implant materials, Kalisz et al. [21] successfully deposited graphene on titanium alloys, resulting in improved mechanical and corrosion properties. Shadi et al. [22] employed plasma spraying to create graphene oxide/fluorapatite/zinc oxide nanocomposite coatings on Ti alloys. Additionally, *h*-BN-reinforced composite coatings on Ti alloys [23,24] and the use of graphene as a reinforcement phase in magnesium alloys [25,26] have been studied. Apart from their usage as protective coatings or fillers in composites, 2D materials can be injected as additives to body fluids [18,27–29]. Given good dispersibility and colloidal stability of the resulting aqueous solution, this may improve the tribological behavior, especially in systems, which highly depend on biofluids with limited renewal capacity (e.g., natural or artificial load-bearing joints). However, to our best knowledge, there is no study on the usage of MXenes as additives in SFs to enhance the wear resistance of artificial implant materials [18].

While some studies have explored the use of 2D materials, such as graphene, in biotribology, a vast realm of 2D materials with promising mechanical and tribological properties remains unexplored [30]. Among these uncharted materials are MXenes, an emerging and continuously growing class of 2D nanomaterials of early transition metal carbides, nitrides, and carbonitrides [31]. MXenes exhibit unique properties, such as a 2D layered structure, strong in-plane bonding, and high surface-to-volume ratios. However, what sets MXenes apart is their enhanced interlayer interactions, encompassing not only van der Waals forces but also electrostatic and intermolecular interactions due to functional surface groups. MXenes offer versatility through the use of different early transition metals and carbon-to-nitrogen ratio adjustments, providing an inherent compositional diversity. These characteristics make MXenes promising candidates for mechanical and tribological applications when applied as coatings [32–35], reinforcement phases [36–38], or lubricant additives [39,40]. The latter is also extendable towards aqueous solutions due to MXenes' inherent hydrophilicity [41,42]. Although $Ti_3C_2T_x$, the most studied member of the MXene family, has received considerable attention [43], other types of MXenes and especially double transition metal MXenes, differentiated by two different transition metals in their structure (e.g. $Mo_2TiC_2T_x$) remain unexplored in tribology. Moreover, there is currently no reported research on MXenes in the context of biotribology [18]. However, Seredych et al. [44] showed that $Ti_3C_2T_x$ and $Mo_2TiC_2T_x$ can be delaminated directly into stable bovine serum albumin solutions, demonstrating that protein solutions can be used as exfoliation agent and stabilization media for MXenes, which enables their potential use in biomedical applications. Moreover, several *in-vitro* and *in-vivo* studies have shown that MXenes at low to moderate concentrations exhibit good biocompatibility and low cytotoxicity [45,46]. These results have created the fundamental base to explore their application in biomedical applications such as drug delivery, tissue engineering, and biosensing [47–50].

To summarize, there is an urgent need to address the limited wear resistance of load-bearing joint implant materials. Traditional metals, such as CoCr alloys, and AM components towards tailor-make patient-specific joint implants tend to generate wear debris over time that lead to adverse reactions in the body. Current research efforts are focused on the development of low-friction, minimal-wear materials, including the exploration of 2D materials. As pointed out in a recent review [18], however, there is a gap in the understanding how these 2D materials can be effectively integrated into joint implants, especially within the context of SF. Additionally, while 2D materials, such as graphene in particular, have been used either as protective coatings or as reinforcement phase in some biotribological studies, there is a substantial unexplored realm of adding 2D nanomaterials to SFs. Namely, some other 2D materials, such as MXenes, which offer unique mechanical and tribological properties, have not been investigated in the context of joint implants and biotribology. Therefore, this contribution seeks to bridge these gaps. We hypothesize that adding 2D MXenes to SFs may help to reduce wear of additively manufactured metal implant materials compared to pure SF lubrication. To this end, we synthesized $Ti_3C_2T_x$ and $Mo_2TiC_2T_x$ MXenes and studied their dispersibility within a simulated body fluid (SBF) at different concentrations as well as their contact angle, surface tension, and viscosity of the resulting colloidal solutions. Furthermore, using CoCr alloy samples fabricated by laser powder bed fusion (LPBF), we studied the interaction of the MXene-SF-solutions with the substrate as well as their effect on friction and wear in reciprocating ball-on-disk experiments.

2. Materials and methods

2.1. Materials

The synthesis of multi-layer $Ti_3C_2T_x$ was carried out using selective etching of the parental Ti_3AlC_2 MAX phase similar to previous step-by-step reports [51]. In short, the Ti_3AlC_2 MAX phase was synthesized by mixing a molar ratio of 2:2.2:1.25 TiC:Al:Ti powders, dry milling them overnight, and firing them in an alumina crucible at 1400 °C for 4 h in a tube furnace using a ramp rate of 3.5 °C/min and de-ramp rate of 5 °C/min. After firing, the MAX block was turned into a powder and immersed in an aqueous acid solution containing 5 wt% HF (from 48 wt % stock) and 7.2 M HCl at 35 °C for 24 h for a total etching solution volume of 30 mL/g MAX. After etching, the powders were rinsed until a pH of 6 was achieved, dried in vacuum overnight, and used as the etched multi-layer Ti_3C_2T powder for tribological testing.

For the synthesis of multi-layer $Mo_2TiC_2T_x$ MXenes, we first made the Mo_2TiAlC_2 MAX phase similar to the Ti_3AlC_2 MAX phase by mixing a molar ratio of 2:1:1.3:2.7 Mo:Ti:Al:C and firing the powder at 1600 °C for 4 h. All other MAX synthesis steps were the same as Ti_3AlC_2. To yield the MXenes, the Mo_2TiAlC_2 MAX powder was added to a solution containing 10 mL/g MAX of stock 48 % stock HF and maintained at a temperature of 55 °C for 96 h. Similarly to $Ti_3C_2T_x$, the obtained dispersions underwent a washing process to neutralize the acid followed by overnight vacuum drying [52].

The 2D MXenes were added in different concentrations to a SBF, which is commercially available from Bio Chemazone, Canada (BZ183). As specified by the supplier, the reagent itself consists of pyrogen-free double deionized water, minerals, amino acids, lipids, phospholipid, serum proteins, glucose, vitamins, albumin, mucoprotein, sialic acid, dipalmitoyl phosphatidylcholine, urea, and hyaluronic acid (HA). The SBF is 0.2 μm filtered, sterile, autoclaved, colorless and odorless, with a pH of 7.4 ± 0.2. For both MXene types, four different concentrations of 0.5, 2, 5, and 20 mg/mL, respectively, (analytical balance, AS 60/220. R2 PLUS) as well as a reference fluid without additives were prepared in their respective Clear Glass Screw Top PerkinElmer vials. Since MXenes tend to agglomerate, dispersion experiments were conducted to ensure the uniform distribution of $Ti_3C_2T_x$ and $Mo_2TiC_2T_x$ within the SBF. To this end, the suspensions were sonicated using a sonicator (Qsonica) with a small-volume probe for 30 min, with 5-second on/off pulses and an amplitude of 40 %. After sonication, the vials were placed in an ultrasonic bath (Isolab) with water for 1 hour at a temperature of 25–30 °C. The bath temperature was maintained constant using ice and by regularly replacing the water.

The substrates were fabricated from medical grade cobalt chromium tungsten (CoCr) powder (GE Remanium Star CL) with a particle size of 10–45 μm processed by LBPF using a MLab 200R unit (General Electric) with a 200 W fiber laser and a pair of galvo scanning mirrors, and f-theta lens, as well as two stepper motor-controlled platform stages. Nine plates with dimensions 20×20×5 mm^3 were printed in a 3 × 3 arrangement on a stainless-steel build plate using a layer height of 0.015 mm, a laser power of 180 W, a speed of 150 cm/s, a hatch spacing of 0.06 mm, and an interlayer rotation scanning pattern. After wire-cutting (Jiangsu Sammlite Machinery), the samples were ground and polished in a multi-step process to achieve a mirror-like finish with S_a values below 40 nm as ensured by white light interferometry (WLI; RTEC MFT-5000).

2.2. Characterization and biotribological testing

To assess the structure of the multi-layer $Ti_3C_2T_x$ and $Mo_2TiC_2T_x$ MXenes after synthesis, transmission electron microscopy (TEM, Tecnai F20, FEI) was utilized employing an acceleration voltage of 200 kV. X-Ray Diffraction (XRD, D8 Advance X-Ray diffractometer, Bruker) using CuKα (λ = 1.5406 Å) radiation was utilized to study the crystalline structure of the as-synthesized $Ti_3C_2T_x$ and $Mo_2TiC_2T_x$ nano-sheets. Irrespective of the studied MXene, the diffractograms were measured within a 2θ range from 5 to 65 ° using a step size of 0.02° s^{-1} in a θ−2θ Bragg-Brentano geometry. Raman spectroscopy (Alpha 300 RA, Witec) was conducted in backscattering geometry using excitation wavelength of 532 nm. For data acquisition, a spectral range between 80 and 1000 cm^{-1} was considered, while using an acquisition time of 128 s/spectrum and a grating of 300 l/mm (spectral resolution of 3 cm^{-1}). Flake size characterization was completed by drop casting MXene single-to-few layer flakes onto a gold-coated alumina substrate and imaging the resultant flakes using a JEOL 7800f field emission scanning electron microscope using an acceleration voltage of 15 kV.

Upon obtaining homogeneous solutions, the vials were placed on a white canvas, and photographs were taken at time intervals of 0, 15, 30, and 60 min as well as after 24, 72, and 168 h using a digital camera (Canon Reflex EOS Rebel t7i) to examine potential settling and dispersion instabilities over time.

Furthermore, contact angle measurements were performed using the sessile drop method at room temperature. Thereby, 2 μL drops of the respective fluids were generated from a syringe (Norm Ject F Luer Solo), carefully dropped on the substrate, illuminated by high power monochromatic LED and captured by a high-speed camera (Krüss DSA25). Five measurements were conducted for each concentration. The surface tension was measured by analyzing the shape of a liquid drop suspended from the tip of a needle. In our case, drops from solutions of varying concentrations and a needle from an 1 mL syringe were used (Norm Ject F Luer Solo; Krüss DSA25). Five repetitions were realized for each concentration.

The dynamic viscosity was measured on a stress-controlled rheometer with a combined motor transducer system (Anton Paar MCR 302) with a Peltier temperature control (C-PTD200) and Peltier-temperature controlled hood (H-PTD 220) in plate-on-plate configuration with disposable plates (D-PP25/AL/S07) of a 25 mm diameter. Thereby, 1 ml of the fluid, which was identified as suitable in preliminary tests, was placed onto the bottom plate using a pipette. Subsequently, the measurement gap of 1 mm was established, and excessive fluid was carefully removed. The shear-rate was varied within a range of 10 1/s to 1000 1/s in 11 logarithmic increments, representing the range relevant to human knee joints [53–55]. Finally, only the initial 10 steps were included in the analysis to avoid any effect of turbulences and measurement deviations at high shear rates on the results. Lower shear rates necessitate a longer time for the rheometer speed control to set and stabilize the desired shear rate, along with performing an adequate number of rotations for data acquisition. To address these challenges, an inverse logarithmic distribution of shear rate and measurement point duration was chosen (10 1/s was held for 10 s and 1000 1/s for 2 s). Each measurement was replicated three times using the same fluid sample with shear rates in an ascending, descending, and then ascending manner (up-down-up) to identify thixotropy or shear-induced degradation. In analogy to [53], temperature encompassed ambient conditions (25 °C) as well as biologically relevant temperatures, i.e., 34, 37, and 40 °C. The shear-rate ramps started after reaching the desired temperature within ±0.1 °C for 2 min. Every temperature level was repeated three times with a new fluid, resulting in a total of nine measurements for each condition.

Friction and wear tests were conducted using a multi-functional tribometer (RTEC MFT-5000) with a 5 μL volume of the different solutions at a normal load of 0.5 N in linear reciprocating sliding conditions for 15 min. Each sliding cycle consisted of 5 mm displacement at a frequency of 1 Hz and an acceleration of 0.1 mm/s^2, i.e. a maximum sliding speed of 5 mm/s. A 4 mm diameter alumina (Al_2O_3) ball was used as the counterbody. All measurements were done in duplicate. The coefficients of friction (COF) were studied in real time and the resulting wear volumes were measured by the integrated WLI (RTEC MFT-5000). After tribo-testing, the samples were completely cleaned in an ultrasonic bath using acetone and ethanol to remove any residues of the SBF and wear debris. Subsequently, the as-formed wear tracks were studied by

optical microscopy (Olympus) and Raman spectroscopy using the aforementioned experimental conditions.

3. Results and discussion

3.1. Characterization

As verified by the TEM micrographs in Fig. 1a and b, the used synthesis approach resulted in well-defined, regular $Ti_3C_2T_x$ and $Mo_2TiC_2T_x$ nano-sheets with a multi-layer nature and interlamellar spacings of about 0.84 and 1.02 nm, respectively. These measured values align well with published literature data in [43,56]. The conducted XRD and Raman analysis, as displayed in Fig. 1c and d, verified the typical diffraction peaks and Raman bands, which align well with their overall stoichiometry as well as the existence of -OH, -O and -F terminations [51,57–59].

Photographic images of the SBF with the addition of different amounts of $Ti_3C_2T_x$ and $Mo_2TiC_2T_x$ at concentrations of 0.5 (magenta), 2 (green), 5 (blue), and 20 mg/mL (gold) directly after the dispersion treatment as well as after 15, 30, and 60 min, respectively, are depicted in Fig. 2a and b. Please note that the color coding for the different concentrations will be kept throughout the manuscript, whereby $Ti_3C_2T_x$ is represented in darker and $Mo_2TiC_2T_x$ in more pastel colors.

Based on Fig. 2, it can be observed that the dispersions turn from fully transparent, over light grey to a dark grey or black color with increasing MXene concentrations. Also. regardless of the type of MXenes and concentration, MXene remained suspended in the solution without settling, thus exhibiting a good dispersion stability, which can be partly attributed to the involved amphiphilic proteins, such as albumin, with large molecule dimensions functioning as a surface ligand [44,60,61]. In addition, we characterized the flake sizes of the MXenes using scanning electron microscopy (SEM) and found that $Ti_3C_2T_x$ and $Mo_2TiC_2T_x$ MXenes demonstrate an average flake size of 5.11 ± 3.17 μm and 0.99 ± 0.51 μm, respectively (Figure S1). Furthermore, the lack of a notable color change over time indicates a slow oxidation rate [62]. This enables the reproducibility of results in both characterization assays and biotribological testing, which ensures that consistent solutions are utilized across various experiments. To assess the dispersion behavior and stability for an extended time, the dispersions for the MXenes with the best friction and wear performance were studied and imaged up to one week. In this regard, the dispersions showed fair stability without any color change, as exemplarily shown in Figure S2.

The mean contact angles and surface tensions for both MXenes dependent on the respective concentration on the additively manufactured CoCr substrates are summarized in Fig. 3a-c. The reference state (the solution without MXenes) exhibited the lowest average contact angle of 59.5° (Fig. 3a). In contrast, the solution with a concentration of 20 mg/mL $Ti_3C_2T_x$, which reflected the highest concentration, presented an averaged contact angle of 76.1° The concentrations of 0.5, 2, and 5 mg/mL demonstrated comparable contact angles with values of 67.5, 66.0, and 65,4°, respectively, whereby error bars do partially overlap. This suggests that the contact angle just increases for higher $Ti_3C_2T_x$ concentrations. Regarding $Mo_2TiC_2T_x$, concentrations of 0.5, 2, and 5 mg/mL presented similar averaged contact angles of 78.4, 73.4, and 77.6°, respectively. With a value of 83.4°, the concentration of 20 mg/mL of $Mo_2TiC_2T_x$ exhibited the highest average contact angle of all samples tested, also confirming the proportional relationship between the contact angle and the MXene concentration. Additionally, it became evident that for all concentrations of both MXenes, the average contact angles are <90° These results indicate that the substrate possesses hydrophilic properties, allowing the solution to disperse, and distribute homogeneously and easily on the solid surface, establishing a strong bond at the interface [63]. This is highly relevant as most 2D nanomaterials, such as graphene or graphene oxides, exhibit low wetting

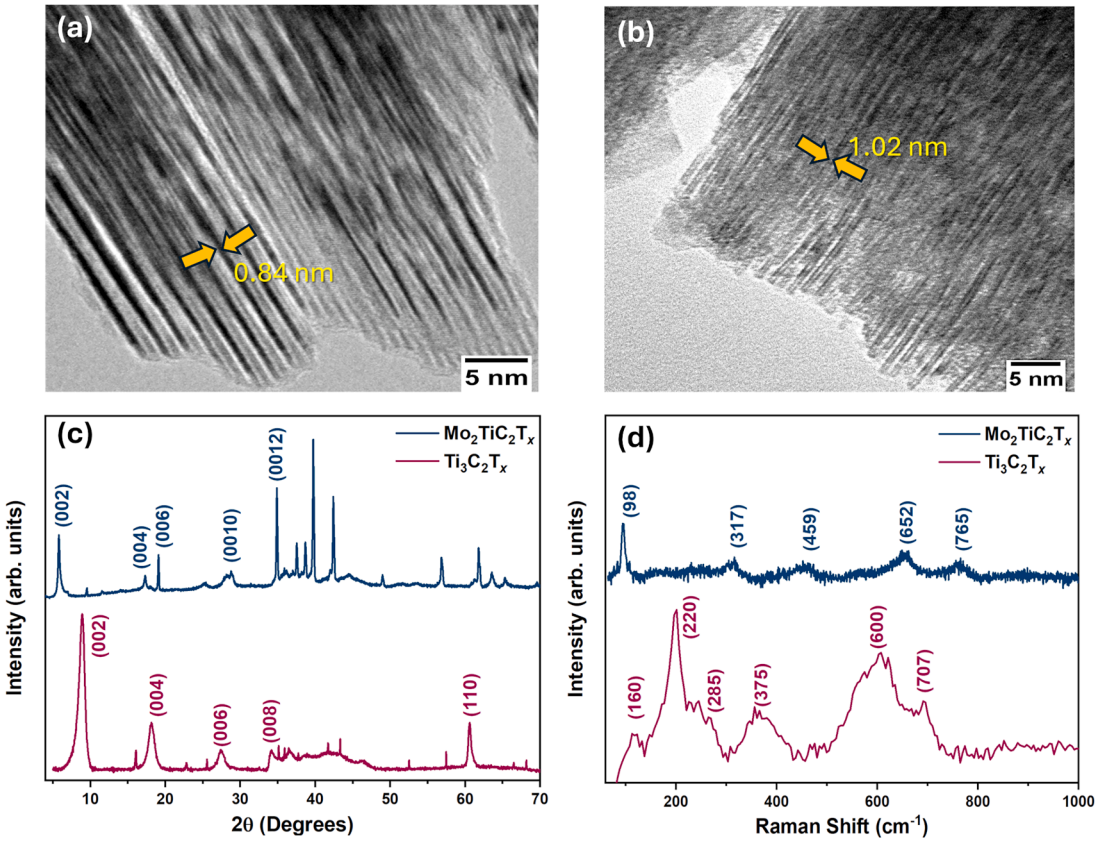

Fig. 1. Transmission electron micrographs of the as-synthesized (a) $Ti_3C_2T_x$ and (b) $Mo_2TiC_2T_x$ nano-sheets with the comparative (c) XRD and (d) Raman analysis.

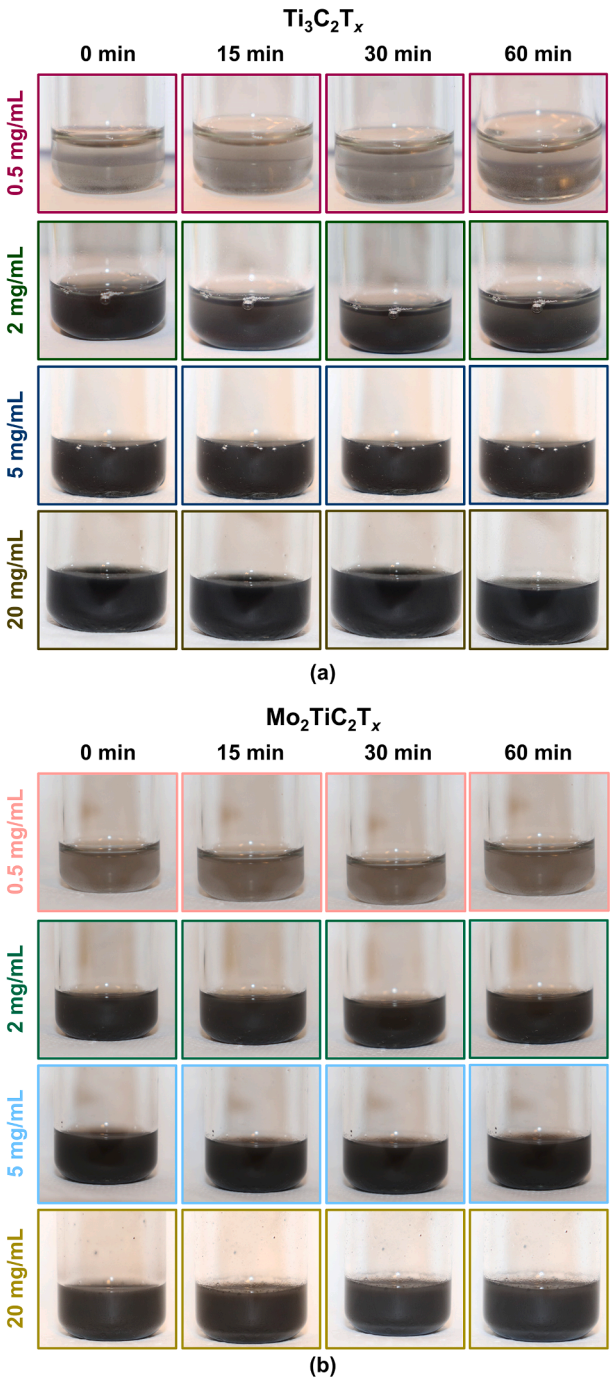

Fig. 2. Photographic images of SBF with the addition of (a) $Ti_3C_2T_x$ and (b) $Mo_2TiC_2T_x$ in concentrations of 0.5, 2, 5, and 20 mg/mL after 0, 15, 30, and 60 min, respectively.

properties in a given matrix due to their hydrophobic nature. Low wetting entails issues such as poor dispersibility, non-uniform distribution, agglomerations, and insufficient bonding at the interface and pores [63]. However, even though all solutions are hydrophilic, the addition of MXenes has a slightly negative effect on the surface wettability of the CoCr substrate. This is evident from the increased contact angle, suggesting that as more MXenes are incorporated, the surface becomes less prone to wetting by the solutions. Overall, these results reveal that the concentration influences the resulting surface wettability of the substrate, which highlights the importance of considering how these wettability changes may affect the subsequent tribological behavior.

Based on Fig. 3c, the surface tension generally followed the opposite trend as the contact angle measurements and the addition of MXenes led to a decrease. While the reference experienced a surface tension of 64.3 mN/m, the lowest values were achieved for 2 and 20 mg/mL $Ti_3C_2T_x$ with values of 50.1 and 50.3 mN/m, respectively. Similarly, the concentrations of 0.5 mg/mL and 5 mg/mL exhibited a surface tension of 55.1 and 54.2 mN/m, respectively. In case of $Mo_2TiC_2T_x$, the surface tensions were 51.9, 56.4, 57.6, and 57.0 mN/m for 0.5, 2, 5, and 20 mg/mL, respectively. Generally, there is a slight tendency for the surface tensions to decrease as the additive concentration increases, which suggests a change in the interaction between the liquid and the substrate surface (please refer to the discussion following the description of viscosity results).

Generally, the SBF exhibited a predominantly Newtonian behavior regardless of the concentration adjusted, showing no dependence on the acting shear rate on the MXene concentration. This somewhat contrasts with healthy natural SF or other SBFs based on bovine serum [53,64]. However, SF from patients in arthritic or diseased joints, especially after revision surgery, tend to become increasingly less non-Newtonian [64]. Furthermore, no effects induced by shearing during the conducted shear rate ramps in accelerating or decelerating mode, as well as no non-reversable effects induced by temperature, were observed. This further highlights the stability of the studied SBF colloidal solutions with MXenes.

The averaged dynamic viscosity of the SBF without and with the addition of $Ti_3C_2T_x$ and $Mo_2TiC_2T_x$ at different concentrations and temperatures of 25, 34, 37, and 40 °C, respectively, are summarized in Fig. 4. In general, the viscosity ranged between 8.3 and 16.2 mPa•s and decreased with increasing temperature, which is slightly above the presented data in [53]. This can be explained by the HA being present in the SBF within our study. In this context, HA is known to increase the resulting viscosity due to restricting the segmental mobility of the hyaluronic chain by local hydrogen bonding, thus allowing water molecules to be better bound and forming a more viscous network [65,66].

By adding MXenes, the viscosities remained within a comparable range, which supports the comparability of the biotribological experiments reported in Section 3.2, as viscosity should not exceptionally impact the lubricant film formation and thus the friction as well as wear behavior. Across different temperatures, the trends for the various MXene concentrations were comparable. Accordingly, viscosity decreased with increasing MXene content, with 0.5 and 2 mg/mL, both for $Ti_3C_2T_x$ and $Mo_2TiC_2T_x$, showing no statistically significant difference compared to the reference.

For both MXenes, 20 mg/mL led to a reduction in viscosity, although the lowest values were observed for 5 mg/mL. To a certain extent, this contrasts reports of MXenes in aqueous solutions [67] or other layered nanomaterials, such as graphene, in SBF [68], for which the viscosity tended to rise with increasing concentration. There are several reasons why MXenes at higher concentrations can decrease the dynamic viscosity of the SBF. Cho et al. [67] showed that the rheological properties of colloidal MXene suspensions can be controlled (i.e., intentional viscosity decrease) by various water-soluble polymers that can absorb on the MXene flakes. Similarly, proteins, such as albumin or HA being present in the used SBF can physically adsorb onto the surface of nanomaterials [69–72], including MXenes [44]. One key aspect of albumin's structure relates to its numerous, charged amino acid residues, particularly acidic and basic residues, which induce an overall negative charge on the protein's surface [73]. This negative charge contributes to albumin's hydrophilic character. HA is a polysaccharide composed of repeating disaccharide units of d-glucuronic acid and N-acetyl-d-glucosamine. Due to carboxyl groups, d-glucuronic acid is negatively charged, which also makes it strongly hydrophilic. Therefore, the protein adsorption onto MXenes flakes is likely to occur through electrostatic interactions, hydrogen bonding, hydrophobic interactions, or specific chemical sites on the MXene surface [44]. Furthermore, MXenes may form complexes with HA or albumin in the fluid environment. By

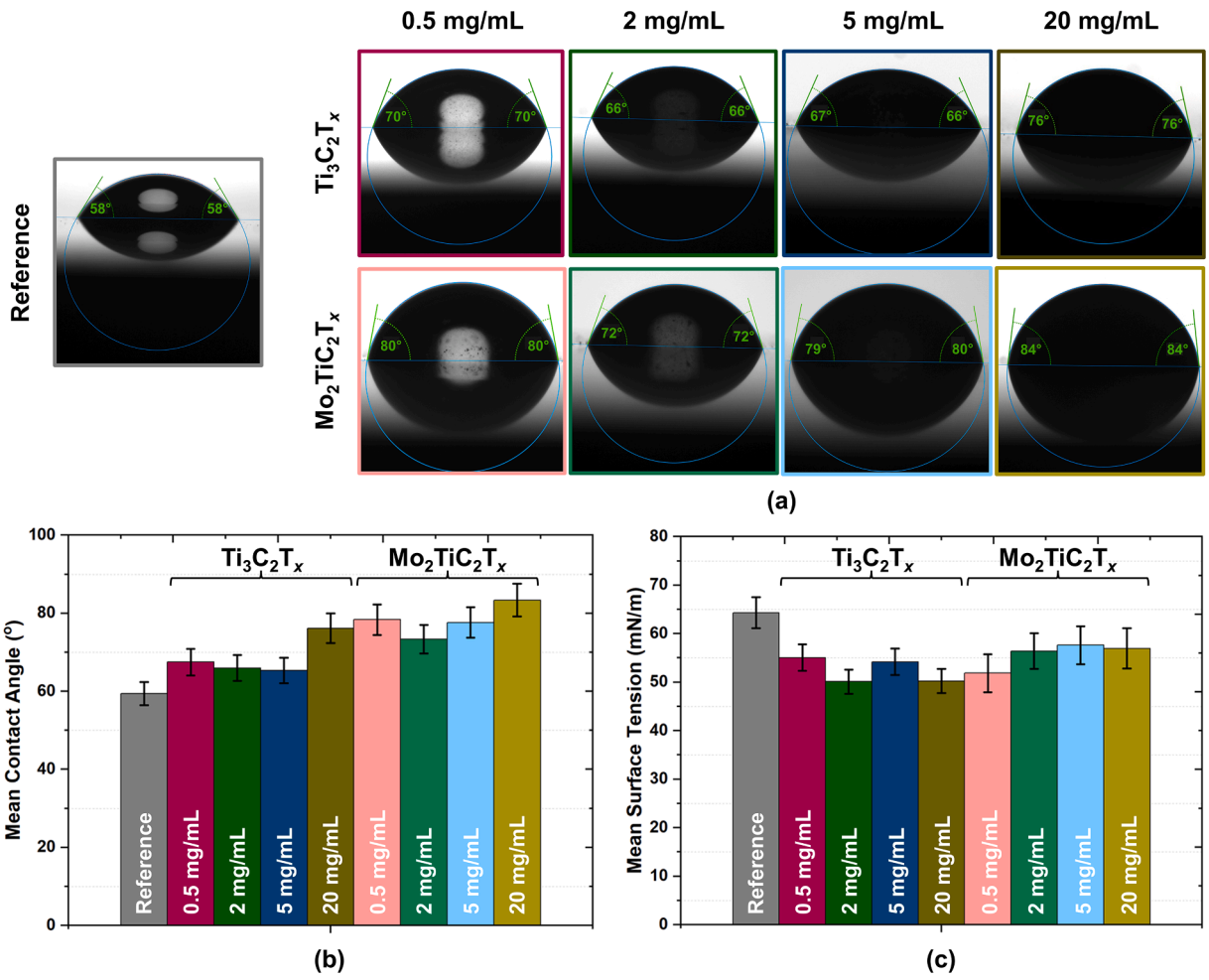

Fig. 3. (a) Representative contact angle measurements, (b) averaged contact angles and (c) surface tension of SBF without and with the addition of $Ti_3C_2T_x$ and $Mo_2TiC_2T_x$ in different concentrations (n = 5). The error bars indicate the calculated standard deviations.

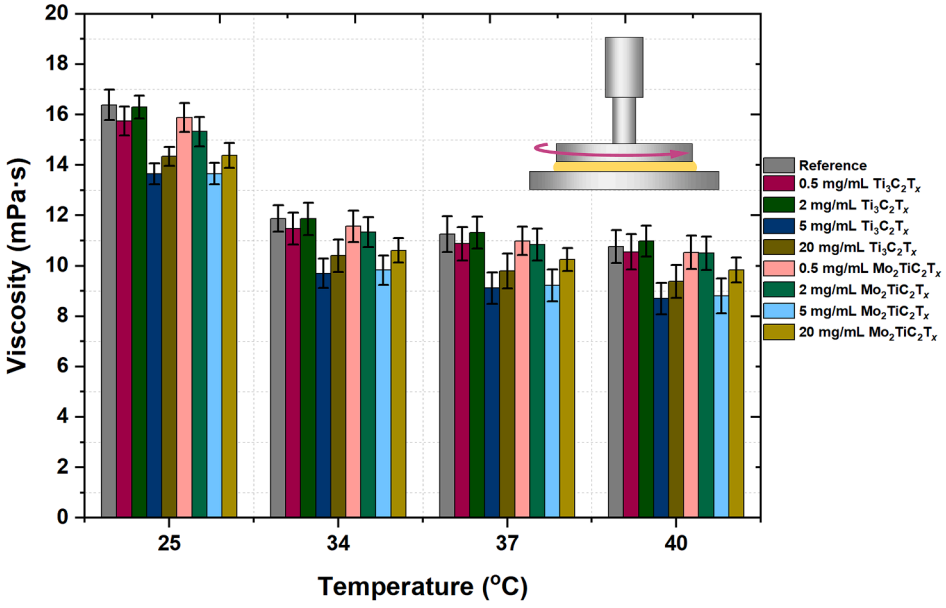

Fig. 4. Averaged dynamic viscosity of SBF without and with the addition of $Ti_3C_2T_x$ and $Mo_2TiC_2T_x$ in different concentrations and at different temperatures (n = 9). The error bars indicate the calculated standard deviations.

interacting with protein aggregates or binding to the protein surface, MXenes could reduce the strength of intermolecular interactions between the biomolecules (e.g., proteins) thus preventing the formation of larger aggregates that contribute to viscosity increase. Finally, MXene nanosheets might promote a smoother fluid flow by reducing friction between adjacent fluid layers. This effect may result from the shear-induced alignment of MXene flakes along the flow direction, facilitating the flow of fluid molecules and reducing the resistance to flow, thereby lowering the resulting viscosity. With a further increase of the MXene concentration to 20 mg/mL, the likelihood of particle-particle interactions also increases. These interactions can result in the formation of particle clusters or agglomerations, which contribute to an increased viscosity by impeding the fluid flow.

3.2. Biotribological behavior

Representative plots of the COF over time as well as the mean COFs averaged over the second half of the sliding time (excluding running-in) are depicted in Fig. 5a and b, respectively. Initially, the tests started with a COF of approximately 0.21. Then, within the first 50 s, the COF of the reference reaches an initial peak of around 0.37, followed by a rapid decrease in the next 100 s. Subsequently, it stabilizes around an average COF of 0.18, while still showing pronounced fluctuations (Fig. 5a). The COFs with MXenes, particularly $Ti_3C_2T_x$, were somewhat more stable, which can also be seen in the reduced standard deviations (Fig. 5b). While the addition of $Mo_2TiC_2T_x$ tended to increase friction compared to the reference, $Ti_3C_2T_x$ at concentrations of 0.5 and 5 mg/mL led to a slight reduction in the COF up to 5 and 9 %, respectively.

The averaged wear coefficient for SBF lubrication without and with the addition of $Ti_3C_2T_x$ and $Mo_2TiC_2T_x$ in different concentrations is displayed in Fig. 6. Thereby, wear when using $Ti_3C_2T_x$ tends to decrease with increasing concentration, with the best performance obtained at a concentration of 5 mg/mL, which also correlated with the lowest viscosity (Fig. 4). Conversely, when using $Mo_2TiC_2T_x$, wear increases with concentration with the best performance shown for 0.5 mg/mL. As previously shown, both types of MXenes resulted in an increase in contact angle, indicating a decreased wettability. The can be favorable for tribological applications as higher contact angles can help to retain the lubricant on the surface, preventing it from spreading too thinly or being displaced under load, which can maintain effective lubrication and reduce wear. In contrast, it was shown that the addition of MXenes slightly decreased the viscosity, which generally is assumed to be not favorable for fluid film formation, load-carrying capacity, and wear protection. Despite the decrease in wettability and viscosity, $Ti_3C_2T_x$

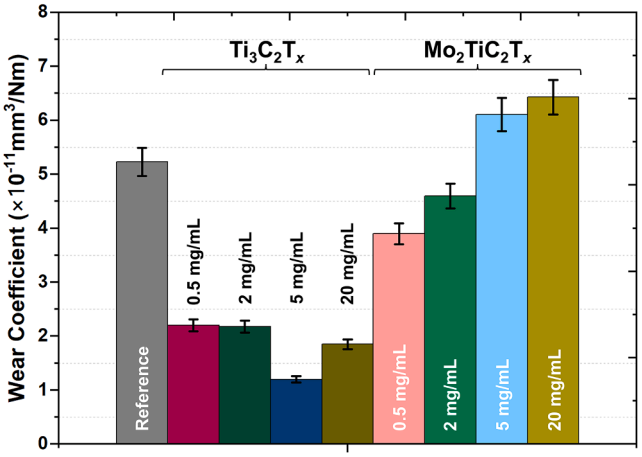

Fig. 6. Averaged wear coefficient for lubrication by SBF without and with the addition of $Ti_3C_2T_x$ and $Mo_2TiC_2T_x$ in different concentrations (n = 2). The error bars indicate the standard deviation.

exhibited wear protection, which implies that other factors, such as the formation of a protective tribo-film observed via Raman spectroscopy, play a more dominant role in reducing wear. Moreover, $Ti_3C_2T_x$ exhibited substantially lower wear rates compared to $Mo_2TiC_2T_x$. In this regard, $Ti_3C_2T_x$ at a concentration of 5 mg/mL showed a wear reduction of 77 %, while $Mo_2TiC_2T_x$ at 0.5 mg/mL merely achieved a wear reduction of 25 %. A possible explanation for the better biotribological performance of $Ti_3C_2T_x$ relates to be its laminar structure and ability to form a lubricious tribofilms on metallic substrates. These films help to reduce the direct contact between rubbing surfaces thus decreasing wear. In contrast, $Mo_2TiC_2T_x$ may have less favorable properties in terms of lubricating film formation under lubricated SFB conditions, resulting in higher friction and wear compared to $Ti_3C_2T_x$.

To shed more light on the involved processes, the formed species in the wear tracks were analyzed by optical microscopy and Raman spectroscopy. For this purpose, the as-tested specimens were fully cleaned in an ultrasonic bath to remove all remaining SBF, formed wear debris and non-attached MXenes.

Even after throughout cleaning, notable reaction products are visible in the wear tracks after tribo-testing as verified in the optical micrographs displayed in Fig. 7a and b. In case of the reference scenario, a wide wear track characterized by notable abrasive marks was displayed in Fig. 7a, alongside Raman signals identifying amorphous carbon

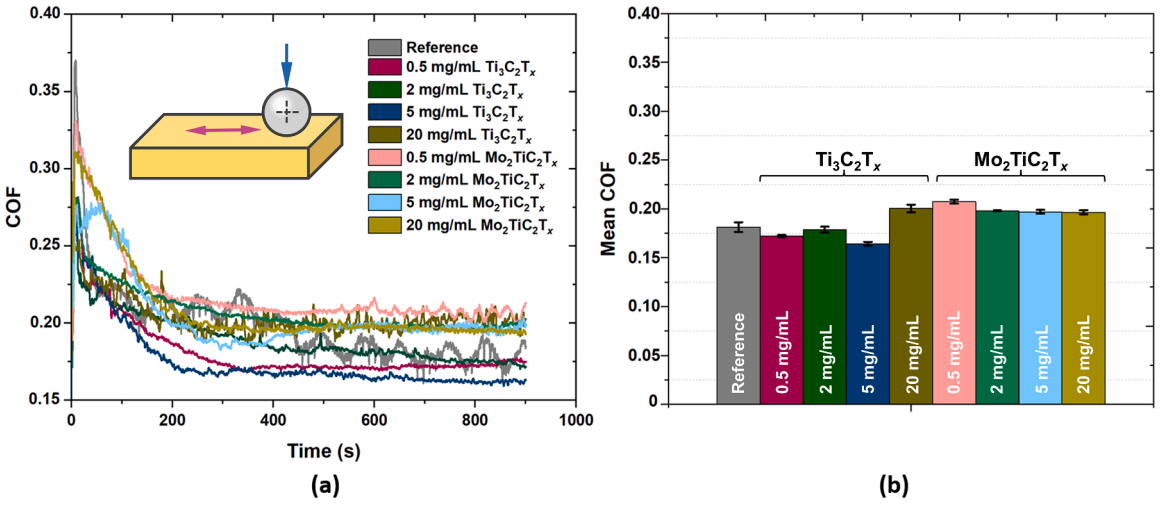

Fig. 5. (a) Representative COF over time and (b) averaged COF for lubrication by SBF without and with the addition of $Ti_3C_2T_x$ and $Mo_2TiC_2T_x$ in different concentrations (n = 2). The error bars indicate the calculated standard deviations.

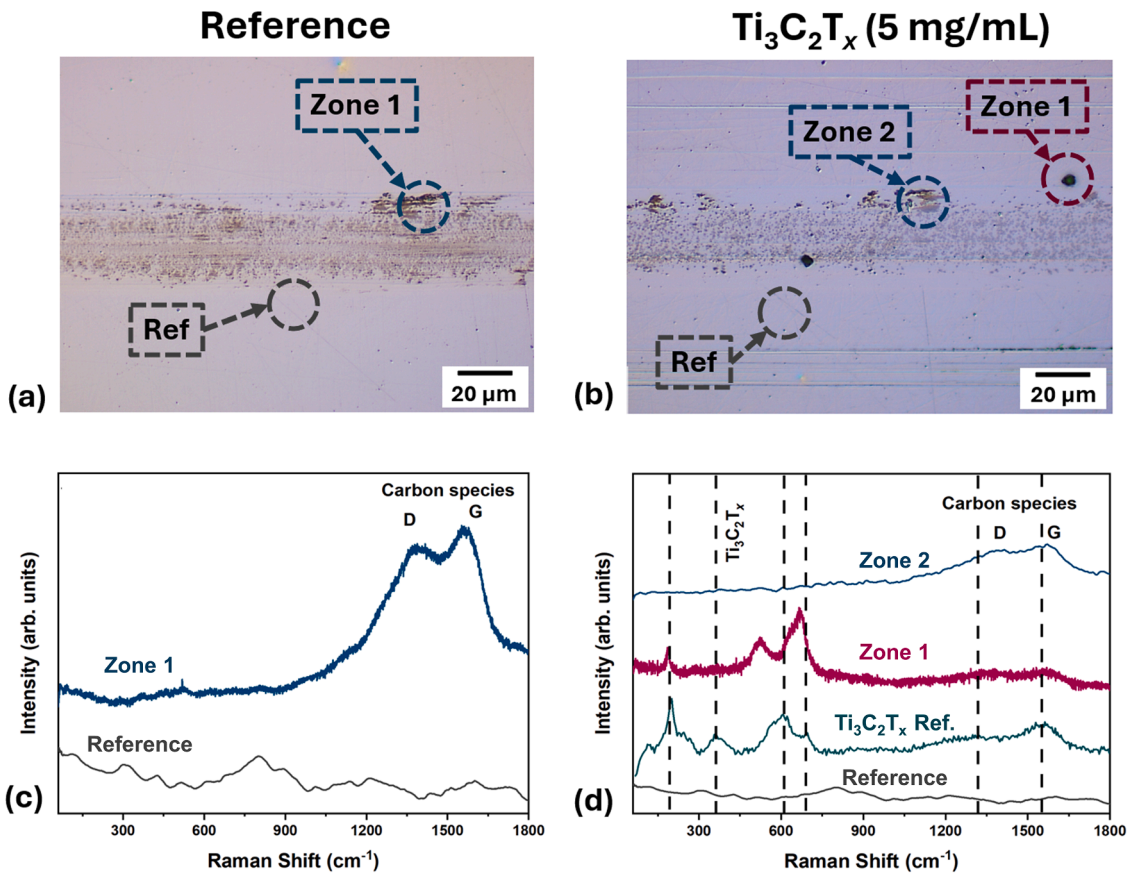

Fig. 7. Optical micrographs of the wear tracks on the CoCr samples after tribo-testing and sample cleaning in the (a) reference case and (b) with 5 mg/mL $Ti_3C_2T_x$ as well as (c, d) Raman analyses at different positions inside and outside the wear track, respectively.

species along the edges of the wear track (Fig. 7c). This can be attributed to abrasive wear processes and frictional heating together with tribo-chemical decomposition of organic molecules present in the SBF, such as amino acids, lipids, and proteins, resulting in the formation of carbonaceous species.

In contrast, a notably different situation emerged for the sample lubricated with 5 mg/mL $Ti_3C_2T_x$ (Fig. 7b). Inside the wear track, a patchy structure became evident, without any pronounced sign of abrasion, which correlates well with the observed wear reduction. As demonstrated in Fig. 7d, the conducted Raman analysis verified again the existence of amorphous carbon (zone 2), which are partially intermixed with spatially separated MXene-related particles/species (zone 1). The observation of these Raman bands, which align well with the initial Raman signal of $Ti_3C_2T_x$, provides clear evidence that MXene nanosheets have been strongly attached to the underlying substrate due rubbing under the involved thermomechanical impact. These findings suggest the development of a wear-protecting tribofilm containing amorphous carbon and MXene species. Due to the verification of amorphous carbon in the reference case, the wear-reducing effect can be clearly assigned to the existence and presence of MXene in the formed tribofilm.

In case of the SBF containing $Mo_2TiC_2T_x$, optical microscopy revealed a different situation irrespective of the tested concentration as evidenced in Figure S3. Pronounced abrasive wear marks (Figure S3 b-f) are clearly observable in the entire wear track, while material accumulations can be found at the reversal points (Figure S3 a, c, d and f). The formed patchy-like structures (similar to the SBF only) were again traced back to amorphous carbon species (not shown here). This is indicative that $Mo_2TiC_2T_x$ did not remain in the tribological interface and got shifted to as well as accumulated at the reversal points. This goes hand in hand with the downgraded wear performance since $Mo_2TiC_2T_x$ was not capable to attach to the underlying substrate to form a lubricious and wear-resistant tribo-film.

4. Conclusions

In conclusion, our investigation sheds light on the biotribological behavior of additively manufactured CoCr substrates when $Ti_3C_2T_x$ and $Mo_2TiC_2T_x$ MXenes are used as additives in a synovial fluid. The results obtained offer significant insights into the potential of MXenes in a biotribological context:

- The observed excellent dispersion stability of MXenes in SBF underscores their suitability for reproducible characterization assays and biotribological testing. This stability is crucial to ensure the consistency in potential clinical application.
- The analysis of the static contact angle and surface tension revealed alterations in substrate wettability upon MXene addition. While the solutions maintained their hydrophilic character, the incorporation of MXenes decreased the resulting surface wettability. This finding underscores the need to consider MXene-induced changes in surface properties when assessing their biotribological performance under lubricated conditions.
- The viscosity analysis demonstrated that the MXene addition generally resulted in a reduced dynamic viscosity, particularly at higher concentrations. This reduction was attributed to the interactions between MXene flakes and the involved biomolecules, such as albumin or HA, which can disrupt intermolecular interactions and promote a smoother fluid flow, ultimately lowering viscosity even at elevated MXene concentrations.
- Regarding the biotribological behavior, $Ti_3C_2T_x$ exhibited more stable coefficients of friction compared to $Mo_2TiC_2T_x$, with

concentrations of and 5 mg/mL showing a slight reduction in friction. Additionally, $Ti_3C_2T_x$ generally led to lower wear rates compared to $Mo_2TiC_2T_x$, with the best concentration found at 5 mg/mL for $Ti_3C_2T_x$ and 0.5 mg/mL for $Mo_2TiC_2T_x$.
- Optical microscopy and Raman spectroscopy revealed significant differences between the wear tracks of the reference and $Ti_3C_2T_x$-lubricated specimens. While the reference exhibited abrasive wear and the formation of amorphous carbon, the wear track of the $Ti_3C_2T_x$-lubricated sample demonstrated no abrasion and less wear as well as the formation of tribo-film consisting of amorphous carbon and MXene-related species, which were firmly attached to the substrate.

Overall, our findings suggest that especially $Ti_3C_2T_x$ hold great promise to mitigate friction and wear in biotribological applications due to their laminar structure and effective lubricating film formation. These findings indicate that the choice of respective MXene type and optimal concentration depends on various factors, while detailed analysis is necessary to determine the most effective combination to reduce wear in specific applications.

Ethical statement

No chemicals, procedures or equipment that have any unusual hazards inherent in their use have been employed. No living animal subjects were involved within this study. The study was conducted in compliance with relevant laws and institutional guidelines as well as in accordance with the Declaration of Helsinki and the Code of Ethics of the World Medical Association.

CRediT authorship contribution statement

Max Marian: Writing – review & editing, Writing – original draft, Visualization, Supervision, Resources, Project administration, Methodology, Investigation, Funding acquisition, Formal analysis, Data curation, Conceptualization. **Cotty D. Quiroz Esteban:** Methodology, Investigation, Formal analysis, Data curation. **Dario F. Zambrano:** Writing – review & editing, Visualization, Investigation. **Sangharatna M. Ramteke:** Writing – review & editing, Visualization, Investigation, Formal analysis, Data curation. **Jorge Ramos Grez:** Writing – review & editing, Resources. **Brian C. Wyatt:** Writing – review & editing, Investigation. **Jacob Patenaude:** Investigation. **Bethany G. Wright:** Investigation. **Babak Anasori:** Writing – review & editing. **Andreas Rosenkranz:** Writing – review & editing, Writing – original draft, Supervision, Methodology, Investigation, Formal analysis, Data curation, Conceptualization.

Declaration of competing interest

The authors declare that they have no known competing financial interests or personal relationships that could have appeared to influence the work reported in this paper.

Data availability

Data will be made available on request.

Acknowledgments

M. Marian greatly acknowledges the financial support from the Vicerrectoría Académica (VRA) of the Pontificia Universidad Católica de Chile within the Programa de Inserción Académica (PIA) as well as from Schaeffler FAG Foundation within the Future Technology Award 2022. S. Ramteke and M. Marian kindly acknowledge the financial support given by ANID-Chile within the project Fondecyt de Postdoctorado N° 3230027. J. Ramos-Grez acknowledges the financial support given by ANID-Chile within the project Fondequip EQM 180081. A. Rosenkranz gratefully acknowledges the financial support of ANID-Chile within the projects Fondecyt Regular 1220331 and Fondequip EQM190057 as well as the Millennium Science Initiative Program (NCN2023_007). B. Anasori and his team are thankful to the support from the US NSF, award number DMR-SSMC 2419026 for the MXene synthesis. Dario F. Zambrano acknowledges the financial support funded by ANID postdoctoral FONDECYT (3220165) and FONDECYT project 1191779.

Supplementary materials

Supplementary material associated with this article can be found, in the online version, at doi:10.1016/j.apmt.2024.102464.

References

[1] M. Marian, R. Shah, B. Gashi, S. Zhang, K. Bhavnani, S. Wartzack, A. Rosenkranz, Exploring the lubrication mechanisms of synovial fluids for joint longevity - A perspective, Colloids Surf. B Biointerfaces 206 (2021) 111926, https://doi.org/10.1016/j.colsurfb.2021.111926.
[2] D. Nečas, M. Marian, Y. Sawae, Lubrication of hip and knee joint replacements: the contribution of experiments and numerical modeling, in: T. Rao, S.B. Kasolang, X. Guoxin, J.K. Katiyar, A. Rani (Eds.), Biotribology: Emerging Technologies and Applications, CRC Press, Boca Raton, Florida, United States, 2021, pp. 33–61.
[3] X. Zhang, Y. Zhang, Z. Jin, A review of the bio-tribology of medical devices, Friction 10 (2022) 4–30, https://doi.org/10.1007/s40544-021-0512-6.
[4] Z.M. Jin, J. Zheng, W. Li, Z.R. Zhou, Tribology of medical devices, Biosurf. Biotribol. 2 (2016) 173–192, https://doi.org/10.1016/j.bsbt.2016.12.001.
[5] R. Shah, B. Gashi, S. Hoque, M. Marian, A. Rosenkranz, Enhancing mechanical and biomedical properties of protheses - Surface and material design, Surf. Interf. 27 (2021) 101498, https://doi.org/10.1016/j.surfin.2021.101498.
[6] J.A. López-López, R.L. Humphriss, A.D. Beswick, H.H.Z. Thom, L.P. Hunt, A. Burston, C.G. Fawsitt, W. Hollingworth, J.P.T. Higgins, N.J. Welton, A.W. Blom, E.M.R. Marques, Choice of implant combinations in total hip replacement: systematic review and network meta-analysis, BMJ 359 (2017) j4651, https://doi.org/10.1136/bmj.j4651.
[7] O. Bazaka, K. Bazaka, P. Kingshott, R.J. Crawford, E.P. Ivanova, C. Spicer, Chapter 1. *Metallic Implants For Biomedical Applications*, The Chemistry of Inorganic Biomaterials, Royal Society of Chemistry, Cambridge, 2021, pp. 1–98.
[8] K.S. KATTI, D. VERMA, D.R. KATTI, Materials for joint replacement. Joint Replacement Technology, Elsevier, 2008, pp. 81–104.
[9] R. Shah, N. Pai, A. Rosenkranz, K. Shirvani, M. Marian, Tribological behavior of additively manufactured metal components, JMMP 6 (2022) 138, https://doi.org/10.3390/jmmp6060138.
[10] J. Sun, S. Du, Application of graphene derivatives and their nanocomposites in tribology and lubrication: a review, RSC Adv. 9 (2019) 40642–40661, https://doi.org/10.1039/C9RA05679C.
[11] M. Marian, D. Berman, A. Rota, R.L. Jackson, A. Rosenkranz, Layered 2D nanomaterials to tailor friction and wear in machine elements—a review, Adv. Mater. Interfaces (2021) 2101622, https://doi.org/10.1002/admi.202101622.
[12] H. Xiao, S. Liu, 2D nanomaterials as lubricant additive: a review, Mater. Des. 135 (2017) 319–332, https://doi.org/10.1016/j.matdes.2017.09.029.
[13] D. Berman, S.A. Deshmukh, S.K.R.S. Sankaranarayanan, A. Erdemir, A.V. Sumant, Friction. Macroscale superlubricity enabled by graphene nanoscroll formation, Science 348 (2015) 1118–1122, https://doi.org/10.1126/science.1262024.
[14] D. Berman, A. Erdemir, Achieving ultralow friction and wear by tribocatalysis: enabled by In-operando formation of nanocarbon films, ACS Nano 15 (2021) 18865–18879, https://doi.org/10.1021/acsnano.1c08170.
[15] L. Liu, Y. Zhang, Y. Qiao, S. Tan, S. Feng, J. Ma, Y. Liu, J. Luo, 2D metal-organic frameworks with square grid structure: a promising new-generation superlubricating material, Nano Today 40 (2021) 101262, https://doi.org/10.1016/j.nantod.2021.101262.
[16] Y. Fu, J. Zhang, H. Lin, A. Mo, 2D titanium carbide(MXene) nanosheets and 1D hydroxyapatite nanowires into free standing nanocomposite membrane: in vitro and in vivo evaluations for bone regeneration, Mater. Sci. Eng. C Mater. Biol. Appl. 118 (2021) 111367, https://doi.org/10.1016/j.msec.2020.111367.
[17] X. Liu, A.L. Miller, S. Park, M.N. George, B.E. Waletzki, H. Xu, A. Terzic, L. Lu, Two-dimensional black phosphorus and graphene oxide nanosheets synergistically enhance cell proliferation and osteogenesis on 3D printed scaffolds, ACS Appl. Mater. Interfaces 11 (2019) 23558–23572, https://doi.org/10.1021/acsami.9b04121.
[18] M. Marian, D. Berman, D. Nečas, N. Emami, A. Ruggiero, A. Rosenkranz, Roadmap for 2D materials in biotribological/biomedical applications - A review, Adv. Colloid Interf. Sci. 307 (2022) 102747, https://doi.org/10.1016/j.cis.2022.102747.
[19] Z. Yuan, B. Tao, Y. He, J. Liu, C. Lin, X. Shen, Y. Ding, Y. Yu, C. Mu, P. Liu, K. Cai, Biocompatible MoS2/PDA-RGD coating on titanium implant with antibacterial property via intrinsic ROS-independent oxidative stress and NIR irradiation, Biomaterials 217 (2019) 119290, https://doi.org/10.1016/j.biomaterials.2019.119290.

[20] C.-Y. Liu, A. Ishigami, T. Kurose, H. Ito, Wear resistance of graphene reinforced ultra-high molecular weight polyethylene nanocomposites prepared by octa-screw extrusion process, Compos. Part B: Eng. 215 (2021) 108810, https://doi.org/10.1016/j.compositesb.2021.108810.
[21] M. Kalisz, M. Grobelny, M. Mazur, M. Zdrojek, D. Wojcieszak, M. Świniarski, J. Judek, D. Kaczmarek, Comparison of mechanical and corrosion properties of graphene monolayer on Ti–Al–V and nanometric Nb2O5 layer on Ti–Al–V alloy for dental implants applications, in: International Conference on Metallurgical Coatings, San Diego 589, 2015, pp. 356–363, https://doi.org/10.1016/j.tsf.2015.05.059, 1989.
[22] S. Salehi, M. Kharaziha, M. Salehi, Multifunctional plasma-sprayed nanocomposite coating based on FA-ZnO-GO with improved bioactivity and wear behaviour, Surf. Coat. Technol. 404 (2020) 126472, https://doi.org/10.1016/j.surfcoat.2020.126472.
[23] A. Tozar, İ.H. Karahan, A comparative study on the effect of collagen and h-BN reinforcement of hydroxyapatite/chitosan biocomposite coatings electrophoretically deposited on Ti-6Al-4V biomedical implants, Surf. Coat. Technol. 340 (2018) 167–176, https://doi.org/10.1016/j.surfcoat.2018.02.034.
[24] A. Tozar, İ.H. Karahan, A comprehensive study on electrophoretic deposition of a novel type of collagen and hexagonal boron nitride reinforced hydroxyapatite/chitosan biocomposite coating, Appl. Surf. Sci. 452 (2018) 322–336, https://doi.org/10.1016/j.apsusc.2018.04.241.
[25] M. Shahin, K. Munir, C. Wen, Y. Li, Nano-tribological behavior of graphene nanoplatelet–reinforced magnesium matrix nanocomposites, J. Magnes. Alloys 9 (2021) 895–909, https://doi.org/10.1016/j.jma.2020.10.001.
[26] M. Shahin, C. Wen, K. Munir, Y. Li, Mechanical and corrosion properties of graphene nanoplatelet–reinforced Mg–Zr and Mg–Zr–Zn matrix nanocomposites for biomedical applications, J. Magnes. Alloys (2021), https://doi.org/10.1016/j.jma.2021.05.011.
[27] W. Qiu, W. Zhao, L. Zhang, H. Wang, N. Li, K. Chen, H. Zhang, Y. Wang, A solid–liquid composite lubricating "nano-snowboard" for long-acting treatment of osteoarthritis, Adv. Funct. Mater. 32 (2022) 2208189, https://doi.org/10.1002/adfm.202208189.
[28] T. Chen, H. Zou, X. Wu, Y. Chen, B. Situ, L. Zheng, G. Yang, Fullerene-like MoS2 nanoparticles as cascade catalysts improving lubricant and antioxidant abilities of artificial synovial fluid, ACS Biomater. Sci. Eng. 5 (2019) 3079–3088, https://doi.org/10.1021/acsbiomaterials.9b00372.
[29] A. Liu, P. Wang, J. Zhang, W. Ye, Q. Wei, Restoration effect and tribological behavior of hyaluronic acid reinforced with graphene oxide in osteoarthritis, J. Nanosci. Nanotechnol. 19 (2019) 91–97, https://doi.org/10.1166/jnn.2019.16443.
[30] A. Rosenkranz, Y. Liu, L. Yang, L. Chen, 2D nano-materials beyond graphene: from synthesis to tribological studies, Appl. Nanosci. 10 (2020) 3353–3388, https://doi.org/10.1007/s13204-020-01466-z.
[31] Y. Gogotsi, B. Anasori, The rise of MXenes, ACS Nano 13 (2019) 8491–8494, https://doi.org/10.1021/acsnano.9b06394.
[32] P.G. Grützmacher, S. Suarez, A. Tolosa, C. Gachot, G. Song, B. Wang, V. Presser, F. Mücklich, B. Anasori, A. Rosenkranz, Superior wear-resistance of Ti3C2Tx multilayer coatings, ACS Nano (2021), https://doi.org/10.1021/acsnano.1c01555.
[33] M. Marian, K. Feile, B. Rothammer, M. Bartz, S. Wartzack, A. Seynstahl, S. Tremmel, S. Krauß, B. Merle, T. Böhm, B. Wang, B.C. Wyatt, B. Anasori, A. Rosenkranz, Ti3C2T solid lubricant coatings in rolling bearings with remarkable performance beyond state-of-the-art materials, Appl. Mater. Today 25 (2021) 101202, https://doi.org/10.1016/j.apmt.2021.101202.
[34] M. Marian, G.C. Song, B. Wang, V.M. Fuenzalida, S. Krauß, B. Merle, S. Tremmel, S. Wartzack, J. Yu, A. Rosenkranz, Effective usage of 2D MXene nanosheets as solid lubricant – Influence of contact pressure and relative humidity, Appl. Surf. Sci. 531 (2020) 147311, https://doi.org/10.1016/j.apsusc.2020.147311.
[35] M. Marian, S. Tremmel, S. Wartzack, G. Song, B. Wang, J. Yu, A. Rosenkranz, MXene nanosheets as an emerging solid lubricant for machine elements – Towards increased energy efficiency and service life, Appl. Surf. Sci. 523 (2020) 1–8, https://doi.org/10.1016/j.apsusc.2020.146503.
[36] M. Malaki, R.S. Varma, Mechanotribological aspects of MXene-reinforced nanocomposites, Adv. Mater. Weinheim. 32 (2020) e2003154, https://doi.org/10.1002/adma.202003154.
[37] J. Hu, S. Li, J. Zhang, Q. Chang, W. Yu, Y. Zhou, Mechanical properties and frictional resistance of Al composites reinforced with Ti3C2T MXene, Chin. Chem. Lett. 31 (2020) 996–999, https://doi.org/10.1016/j.cclet.2019.09.004.
[38] H. Zhang, L. Wang, Q. Chen, P. Li, A. Zhou, X. Cao, Q. Hu, Preparation, mechanical and anti-friction performance of MXene/polymer composites, Mater. Des. 92 (2016) 682–689, https://doi.org/10.1016/j.matdes.2015.12.084.
[39] X. Zhang, Y. Guo, Y. Li, Y. Liu, S. Dong, Preparation and tribological properties of potassium titanate-Ti3C2Tx nanocomposites as additives in base oil, Chin. Chem. Lett. 30 (2019) 502–504, https://doi.org/10.1016/j.cclet.2018.07.007.
[40] M. Xue, Z. Wang, F. Yuan, X. Zhang, W. Wei, H. Tang, C. Li, Preparation of TiO 2 /Ti 3 C 2 T x hybrid nanocomposites and their tribological properties as base oil lubricant additives, RSC Adv. 7 (2017) 4312–4319, https://doi.org/10.1039/C6RA27653A.
[41] H.T. Nguyen, K.-H. Chung, Assessment of tribological properties of Ti3C2 as a water-based lubricant additive, Materials (Basel) 13 (2020) 5545, https://doi.org/10.3390/ma13235545.
[42] H. Cheng, W. Zhao, Regulating the Nb2C nanosheets with different degrees of oxidation in water lubricated sliding toward an excellent tribological performance, Friction 10 (2022) 398–410, https://doi.org/10.1007/s40544-020-0469-x.
[43] B.C. Wyatt, A. Rosenkranz, B. Anasori, 2D MXenes: tunable mechanical and tribological properties, Adv. Mater. Weinheim (2021) e2007973, https://doi.org/10.1002/adma.202007973.
[44] M. Seredych, K. Maleski, T.S. Mathis, Y. Gogotsi, Delamination of MXenes using bovine serum albumin, Colloids Surf. A 641 (2022) 128580, https://doi.org/10.1016/j.colsurfa.2022.128580.
[45] G.P. Lim, C.F. Soon, N.L. Ma, M. Morsin, N. Nayan, M.K. Ahmad, K.S. Tee, Cytotoxicity of MXene-based nanomaterials for biomedical applications: a mini review, Environ. Res. 201 (2021) 111592, https://doi.org/10.1016/j.envres.2021.111592.
[46] S. Sagadevan, W.-C. Oh, Comprehensive utilization and biomedical application of MXenes - A systematic review of cytotoxicity and biocompatibility, J. Drug. Deliv. Sci. Technol. 85 (2023) 104569, https://doi.org/10.1016/j.jddst.2023.104569.
[47] G. Yang, F. Liu, J. Zhao, L. Fu, Y. Gu, L. Qu, C. Zhu, J.-J. Zhu, Y. Lin, MXenes-based nanomaterials for biosensing and biomedicine, Coord. Chem. Rev. 479 (2023) 215002, https://doi.org/10.1016/j.ccr.2022.215002.
[48] S.S. Siwal, H. Kaur, G. Chauhan, V.K. Thakur, MXene-based nanomaterials for biomedical applications: healthier substitute materials for the future, Adv. NanoBiomed Res. 3 (2023) 2200123, https://doi.org/10.1002/anbr.202200123.
[49] I.-C. Lee, Y.-C.E. Li, J.L. Thomas, M.-H. Lee, H.-Y. Lin, Recent advances using MXenes in biomedical applications, Mater. Horiz. 11 (2024) 876–902, https://doi.org/10.1039/D3MH01588B.
[50] S.S. Sana, M. Santhamoorthy, R. Haldar, C.J. Raorane, S. Iravani, R.S. Varma, S.-C. Kim, Recent advances on MXene-based hydrogels for antibacterial and drug delivery applications, Process Biochem. 132 (2023) 200–220, https://doi.org/10.1016/j.procbio.2023.06.022.
[51] A. Thakur, N. Chandran B S, K. Davidson, A. Bedford, H. Fang, Y. Im, V. Kanduri, B. C. Wyatt, S.K. Nemani, V. Poliukhova, R. Kumar, Z. Fakhraai, B. Anasori, Step-by-step guide for synthesis and delamination of Ti3 C2 Tx MXene, Small. Methods 7 (2023) e2300030, https://doi.org/10.1002/smtd.202300030.
[52] K.R.G. Lim, M. Shekhirev, B.C. Wyatt, B. Anasori, Y. Gogotsi, Z.W. Seh, Fundamentals of MXene synthesis, Nat. Synth 1 (2022) 601–614, https://doi.org/10.1038/s44160-022-00104-6.
[53] B. Rothammer, M. Marian, F. Rummel, S. Schroeder, M. Uhler, J.P. Kretzer, S. Tremmel, S. Wartzack, Rheological behavior of an artificial synovial fluid - influence of temperature, shear rate and pressure, J. Mech. Behav. Biomed. Mater. 115 (2021) 104278, https://doi.org/10.1016/j.jmbbm.2020.104278.
[54] M. Nicholls, A. Manjoo, P. Shaw, F. Niazi, J. Rosen, A Comparison between rheological properties of intra-articular hyaluronic acid preparations and reported human synovial fluid, Adv. Ther. 35 (2018) 523–530, https://doi.org/10.1007/s12325-018-0688-y.
[55] D. Prekasan, K.K. Saju, Tribological effectiveness of viscosupplements for osteoarthritis in knee joint, SN Appl. Sci. 1 (2019) 1582, https://doi.org/10.1007/s42452-019-1030-2.
[56] A. Lipatov, H. Lu, M. Alhabeb, B. Anasori, A. Gruverman, Y. Gogotsi, A. Sinitskii, Elastic properties of 2D Ti3C2T x MXene monolayers and bilayers, Sci. Adv. 4 (2018) eaat0491, https://doi.org/10.1126/sciadv.aat0491.
[57] B. Anasori, Y. Xie, M. Beidaghi, J. Lu, B.C. Hosler, L. Hultman, P.R.C. Kent, Y. Gogotsi, M.W. Barsoum, Two-dimensional, ordered, double transition metals carbides (MXenes), ACS Nano 9 (2015) 9507–9516, https://doi.org/10.1021/acsnano.5b03591.
[58] K. Shevchuk, A. Sarycheva, C.E. Shuck, Y. Gogotsi, Raman spectroscopy characterization of 2D carbide and carbonitride MXenes, Chem. Mater. 35 (2023) 8239–8247, https://doi.org/10.1021/acs.chemmater.3c01742.
[59] A. Sarycheva, Y. Gogotsi, Raman spectroscopy analysis of the structure and surface chemistry of Ti 3 C 2 T x MXene, Chem. Mater. 32 (2020) 3480–3488, https://doi.org/10.1021/acs.chemmater.0c00359.
[60] K. Maleski, V.N. Mochalin, Y. Gogotsi, Dispersions of two-dimensional titanium carbide MXene in organic solvents, Chem. Mater. 29 (2017) 1632–1640, https://doi.org/10.1021/acs.chemmater.6b04830.
[61] A.K. Wright, M.R. Thompson, Hydrodynamic structure of bovine serum albumin determined by transient electric birefringence, Biophys. J. 15 (1975) 137–141, https://doi.org/10.1016/S0006-3495(75)85797-3.
[62] C.J. Zhang, S. Pinilla, N. McEvoy, C.P. Cullen, B. Anasori, E. Long, S.-H. Park, A. Seral-Ascaso, A. Shmeliov, D. Krishnan, C. Morant, X. Liu, G.S. Duesberg, Y. Gogotsi, V. Nicolosi, Oxidation stability of colloidal two-dimensional titanium carbides (MXenes), Chem. Mater. 29 (2017) 4848–4856, https://doi.org/10.1021/acs.chemmater.7b00745.
[63] M. Malaki, R.S. Varma, Wetting of MXenes and Beyond, Nanomicro. Lett. 15 (2023) 116, https://doi.org/10.1007/s40820-023-01049-x.
[64] D. Mazzucco, G. McKinley, R.D. Scott, M. Spector, Rheology of joint fluid in total knee arthroplasty patients, J. Orthop. Res. 20 (2002) 1157–1163, https://doi.org/10.1016/S0736-0266(02)00050-5.
[65] J.-H. Zhang, Artificial Synovial Fluid, in: Q.J. Wang, Y.-W. Chung (Eds.), Encyclopedia of Tribology, Springer US, Boston, MA, 2013, pp. 110–113.
[66] T.C. Laurent, U.B. Laurent, J.R. Fraser, The structure and function of hyaluronan: an overview, Immunol. Cell Biol. 74 (1996) A1–A7, https://doi.org/10.1038/icb.1996.32.
[67] H. Cho, S. Lim, G. Kim, J. Park, S. Kim, S.Y. Ryu, S. Kang, H.H. Lee, J. Lee, Control of the rheological properties of concentrated aqueous MXene sediment suspensions using polymeric additives, Colloid. Polym. Sci. 301 (2023) 357–370, https://doi.org/10.1007/s00396-023-05076-3.
[68] A. Cerpa-Naranjo, J. Pérez-Piñeiro, P. Navajas-Chocarro, M.P. Arce, I. Lado-Touriño, N. Barrios-Bermúdez, R. Moreno, M.L. Rojas-Cervantes, Rheological properties of different graphene nanomaterials in biological media, Materials (Basel) (2022) 15, https://doi.org/10.3390/ma15103593.

[69] G. Guan, S. Zhang, S. Liu, Y. Cai, M. Low, C.P. Teng, I.Y. Phang, Y. Cheng, K. L. Duei, B.M. Srinivasan, Y. Zheng, Y.-W. Zhang, M.-Y. Han, Protein induces layer-by-layer exfoliation of transition metal dichalcogenides, J. Am. Chem. Soc. 137 (2015) 6152–6155, https://doi.org/10.1021/jacs.5b02780.
[70] G. Guan, J. Xia, S. Liu, Y. Cheng, S. Bai, S.Y. Tee, Y.-W. Zhang, M.-Y. Han, Electrostatic-driven exfoliation and hybridization of 2D nanomaterials, Adv. Mater. Weinheim. (2017) 29, https://doi.org/10.1002/adma.201700326.
[71] S. Ahadian, M. Estili, V.J. Surya, J. Ramón-Azcón, X. Liang, H. Shiku, M. Ramalingam, T. Matsue, Y. Sakka, H. Bae, K. Nakajima, Y. Kawazoe, A. Khademhosseini, Facile and green production of aqueous graphene dispersions for biomedical applications, Nanoscale 7 (2015) 6436–6443, https://doi.org/10.1039/c4nr07569b.
[72] H. Tao, Y. Zhang, Y. Gao, Z. Sun, C. Yan, J. Texter, Scalable exfoliation and dispersion of two-dimensional materials - an update, Phys. Chem. Chem. Phys. 19 (2017) 921–960, https://doi.org/10.1039/c6cp06813h.
[73] K.A. Majorek, P.J. Porebski, A. Dayal, M.D. Zimmerman, K. Jablonska, A. J. Stewart, M. Chruszcz, W. Minor, Structural and immunologic characterization of bovine, horse, and rabbit serum albumins, Mol. Immunol. 52 (2012) 174–182, https://doi.org/10.1016/j.molimm.2012.05.011.